ARTICLE

doi:10.1038/nature13702

Neutrinos from the primary proton–proton fusion process in the Sun

Borexino Collaboration*

In the core of the Sun, energy is released through sequences of nuclear reactions that convert hydrogen into helium. The primary reaction is thought to be the fusion of two protons with the emission of a low-energy neutrino. These so-called *pp* neutrinos constitute nearly the entirety of the solar neutrino flux, vastly outnumbering those emitted in the reactions that follow. Although solar neutrinos from secondary processes have been observed, proving the nuclear origin of the Sun's energy and contributing to the discovery of neutrino oscillations, those from proton–proton fusion have hitherto eluded direct detection. Here we report spectral observations of *pp* neutrinos, demonstrating that about 99 per cent of the power of the Sun, 3.84×10^{33} ergs per second, is generated by the proton–proton fusion process.

We have known for 75 years that the energy generated by stars comes from the fusion of light nuclei into heavier ones[1–3]. In the Sun, hydrogen is transformed into helium predominantly via the *pp* cycle[4,5], a chain of reactions releasing 26.73 MeV and electron neutrinos ν_e, and summarized as

$$4p \rightarrow {}^4\mathrm{He} + 2e^+ + 2\nu_e$$

The cycle begins with the fusion of two protons into a deuteron, which occurs 99.76% of the time[6] by means of the primary reaction

$$p + p \rightarrow {}^2\mathrm{H} + e^+ + \nu_e$$

Neutrinos produced in this step are referred to as *pp* neutrinos. Some of the nuclear reactions that follow also produce neutrinos of various energies. ^{4}He may also be formed through the CNO (carbon–nitrogen–oxygen) cycle[2], which is thought to be predominant in heavy stars, but to produce at most 1% of the Sun's energy[7,8]. Present models of the Sun[9] precisely predict the flux and energy distribution of emitted neutrinos (Fig. 1). So far, only the radiochemical gallium experiments (after the first observation by GALLEX[10,11] and, later, by SAGE[12]) have been sensitive to *pp* solar neutrinos ($0 < E < 420$ keV). However, by measuring only an integrated flux of all solar electron neutrinos above an energy threshold (233 keV), the *pp* neutrino flux could be extracted only indirectly, by combining the GALLEX and SAGE measurements with those of other experiments[13–17].

The Borexino experiment came online in 2007 with high sensitivity to all solar neutrino components, particularly those below 2 MeV (Fig. 1). Borexino has made the first measurement of ^{7}Be neutrinos[17] and proton–electron–proton (*pep*) neutrinos[18], measured ^{8}B neutrinos[19] at a lower energy threshold than other experiments, and set the best available limit on the solar CNO neutrino component[18]. The detection of *pep* neutrinos itself indirectly indicates the existence of *pp* neutrinos, because the $p + e + p \rightarrow {}^2\mathrm{H} + \nu_e$ reaction is a rare (0.24%; ref. 6) alternative first step of the *pp* cycle. Attempts to measure *pp* neutrinos directly over the past 30 years (see ref. 20 for a recent review) have been hindered by the inability to sufficiently suppress radioactive backgrounds in this low-energy region. The Borexino detector, which is designed to minimize backgrounds from radioactive isotopes both within, and external to, the liquid scintillator target, made it possible to search for the very low-energy *pp* neutrinos. The measured solar *pp* neutrino flux is $(6.6 \pm 0.7) \times 10^{10}$ cm^{-2} s^{-1}, in good agreement with the prediction of the standard solar model[9] (SSM) ($5.98 \times (1 \pm 0.006) \times 10^{10}$ cm^{-2} s^{-1}).

The observation of *pp* neutrinos provides us with a direct glimpse at the keystone fusion process that keeps the Sun shining and strongly reinforces our theories on the origin of almost the entirety of the Sun's energy. Their measured flux can also be used to infer the total energy radiated by the Sun, 3.84×10^{33} erg s^{-1}. However, because photons produced in the Sun's core take a very long time (at least a hundred thousand years; ref. 21) to reach the surface, neutrino and optical observations in combination provide experimental confirmation that the Sun has been in thermodynamic equilibrium over such a timescale.

Searching for *pp* neutrinos with Borexino

The Borexino experiment (Methods) detects solar neutrinos by measuring the energy deposited in the liquid scintillator target by recoiling electrons undergoing neutrino–electron elastic scattering:

$$\nu_x + e \rightarrow \nu_x + e \quad (1)$$

where x denotes one of the three neutrino flavours (e, μ, τ). The detector is fully described in ref. 22.

The solar neutrino flux reaching the Earth is composed not only of electron neutrinos produced in the nuclear reactions in the Sun, but, owing to the process of flavour oscillations (Methods), also of muon and tau neutrinos. The *pp* neutrino energy spectrum extends up to 420 keV, yielding a maximum electron recoil energy of $E_{\mathrm{max}} = 264$ keV (ref. 23). The expected flux of *pp* neutrinos is calculated in the framework of the SSM (Methods). The most recent calculations are those of ref. 9 (other models, such as the one described in ref. 24, give similar results). The predictions for the total flux of *pp* neutrinos at Earth[9] range between $5.98 \times (1 \pm 0.006) \times 10^{10}$ cm^{-2} s^{-1}, for the high-metallicity model, and $6.03 \times (1 \pm 0.006) \times 10^{10}$ cm^{-2} s^{-1}, for the low-metallicity model. The latest values of the neutrino oscillation parameters[25] are needed to calculate the relative proportions of the three flavours within the solar neutrino flux at Earth. For reference, when combining them with the high-metallicity SSM prediction (assumed throughout this paper unless otherwise specified) and using neutrino–electron scattering cross-sections derived from refs 25, 26 (also P. Langacker and J. Erler, personal communication), we expect the *pp* neutrino interaction

*Lists of participants and their affiliations appear at the end of the paper.

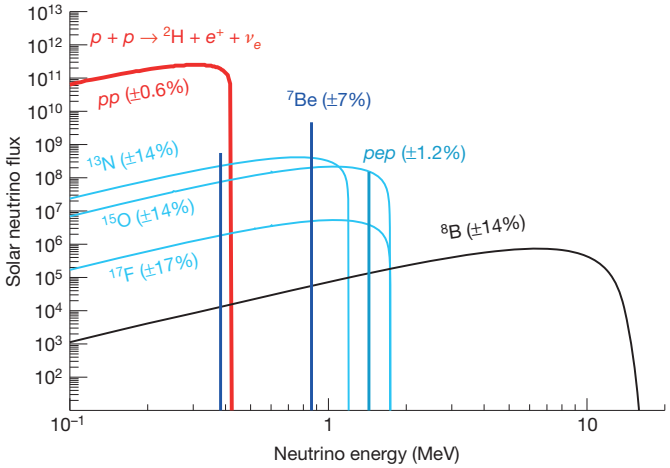

Figure 1 | Solar neutrino energy spectrum. The flux (vertical scale) is given in $cm^{-2}\,s^{-1}\,MeV^{-1}$ for continuum sources and in $cm^{-2}\,s^{-1}$ for mono-energetic ones. The quoted uncertainties are from the SSM[9].

(equation (1)) rate to be 131 ± 2 counts per day (c.p.d.) per 100 t of target scintillator.

The scintillation light generated by a 100 keV event typically induces signals in ~50 photomultiplier tubes (PMTs). This allows for a low detection threshold (~50 keV), much less than the maximum electron recoil energy of *pp* neutrinos (E_{max} = 264 keV).

The *pp* neutrino analysis is performed through a fit of the energy distribution of events selected to maximize the signal-to-background ratio. The selection criteria (Methods) remove residual cosmic muons, decays of muon-produced isotopes, and electronic noise events. Furthermore, to suppress background radiation from external detector components, only events whose position is reconstructed inside the central detector volume (the 'fiducial volume': 86 m^3, 75.5 t) are used in the analysis. The fit is done within a chosen energy interval and includes all relevant solar neutrino components and those from various backgrounds, mostly from residual radioactivity traces dissolved in the scintillator.

Figure 2 shows a calculation of the spectral shape of the *pp* neutrino signal (thick red line), as well as of the other solar neutrino components (^{7}Be, *pep* and CNO), and of the relevant backgrounds (^{14}C, intrinsic to the organic liquid scintillator; its 'pile-up' (see definition below); ^{210}Bi; ^{210}Po; ^{85}Kr; and ^{214}Pb), all approximately at the observed rates in the data. The *pp* neutrino spectral component is clearly distinguished from those of ^{85}Kr, ^{210}Bi, CNO and ^{7}Be, all of which have flat spectral shapes in the energy region of the fit. Most of the *pp* neutrino events are buried

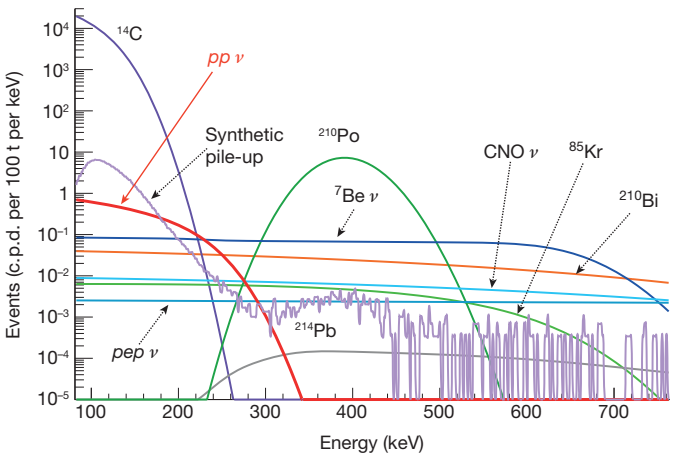

Figure 2 | Energy spectra for all the solar neutrino and radioactive background components. All components are obtained from analytical expressions, validated by Monte Carlo simulations, with the exception of the synthetic pile-up, which is constructed from data (see text for details).

under the vastly more abundant ^{14}C, which is a β-emitter with a *Q* value of 156 keV. In spite of its tiny isotopic fraction in the Borexino scintillator ($^{14}C/^{12}C \approx 2.7 \times 10^{-18}$), ^{14}C β-decay is responsible for most of the detector triggering rate (~30 counts s^{-1} at our chosen trigger threshold). The ^{14}C and *pp* neutrino energy spectra are, however, distinguishable in the energy interval of interest.

The ^{14}C rate was determined independently from the main analysis, by looking at a sample of data in which the event causing the trigger is followed by a second event within the acquisition time window of 16 μs. This second event, which is predominantly due to ^{14}C, does not suffer from hardware trigger-threshold effects and can thus be used to study the rate and the spectral shape of this contaminant. We measure a ^{14}C rate of 40 ± 1 Bq per 100 t. The error accounts for systematic effects due to detector response stability in time, uncertainty in the ^{14}C spectral shape[27], and fit conditions (Methods).

An important consideration in this analysis were the pile-up events: occurrences of two uncorrelated events so closely in time that they cannot be separated and are measured as a single event. Figure 2 shows the expected pile-up spectral shape, which is similar to that of the *pp* neutrinos. Fortunately, the pile-up component can be determined independently, using a data-driven method, which we call 'synthetic pile-up' (Methods). This method provides the spectral shape and the rate of the pile-up component, and is constructed as follows. Real triggered events without any selection cuts are artificially overlapped with random data samples. The combined synthetic events are selected and reconstructed using the same procedure applied to the regular data. Thus, some systematic effects, such as the position reconstruction of pile-up events, are automatically taken into account. The synthetic pile-up is mainly due to the overlap of two ^{14}C events, but includes all possible event combinations, for example ^{14}C with the external background, PMT dark noise or ^{210}Po. ^{14}C–^{14}C events dominate the synthetic pile-up spectrum between approximately 160 and 265 keV. The fit to the ^{14}C–^{14}C pile-up analytical shape in this energy region gives a total rate for ^{14}C–^{14}C pile-up events of 154 ± 10 c.p.d. per 100 t in the whole spectrum, without threshold.

Measurement of the *pp* neutrino flux

The data used for this analysis were acquired from January 2012 to May 2013 (408 days of data; Borexino Phase 2). This is the purest data set available, and was obtained after an extensive purification campaign that was performed in 2010 and 2011[28] and reduced, in particular, the content of ^{85}Kr and ^{210}Bi isotopes, which are important backgrounds in the low-energy region.

The *pp* neutrino rate has been extracted by fitting the measured energy spectrum of the selected events in the 165–590 keV energy window with the expected spectra of the signal and background components. The energy scale in units of kiloelectronvolts is determined from the number of struck PMTs, using a combination of calibration data collected with radioactive sources deployed inside the scintillator[29] and a detailed Monte Carlo model[28].

The fit is done with a software tool developed for previous Borexino measurements[28] and improved for this analysis to include the description of the response of the scintillator to mono-energetic electrons, to give high statistics; a modified description of the scintillation linewidth at low energy, providing the appropriate response functions widths for α- and β-particles (mainly from the ^{210}Po and ^{14}C backgrounds); and the introduction of the synthetic pile-up.

The main components of the fit are the solar neutrino signal (the dominant *pp* component and the low-energy parts of the ^{7}Be, *pep* and CNO components); the dominant ^{14}C background and the associated pile-up; and other identified radioactive backgrounds (^{85}Kr, ^{210}Bi, ^{210}Po and ^{214}Pb). The free fit parameters are the rates of the *pp* solar neutrinos and of the ^{85}Kr, ^{210}Bi and ^{210}Po backgrounds. The ^{7}Be neutrino rate is constrained at the measured value[17] within the error, and *pep* and CNO neutrino contributions are fixed at the levels of the SSM[9], taking into account the values of the neutrino oscillation parameters[25]. The ^{14}C and the synthetic pile-up rates are determined from the data

independently and fixed in the fit, allowing for a variation consistent with their measured uncertainty. The ^{214}Pb rate is fixed by the measured rate of fast, time-correlated ^{214}Bi(β)–^{214}Po(α) coincidences. The scintillator light yield and two energy resolution parameters are left free in the fit.

The energy spectrum with the best-fit components is shown in Fig. 3. The corresponding values of the fitted parameters are given in Table 1.

Many fits have been performed with slightly different conditions to estimate the robustness of the analysis procedure. In particular, we varied the energy estimator, the fit energy range, the data selection criteria and the pile-up evaluation method (Methods). The root mean square of the distribution of all the fits is our best estimate of the systematic error (7%). In addition, a systematic uncertainty (2%) due to the nominal fiducial mass determination is added in quadrature; this was obtained from calibration data by comparing the reconstructed and nominal positions of a (^{222}Rn–^{14}C) radioactive source located near the border of the fiducial volume[29]. Other possible sources of systematic errors, like the dependence of the result on the details of the energy scale definition and on the uncertainties in the ^{14}C and ^{210}Bi β-decay shape factors, were investigated and found to be negligible (Methods). We also verified that varying the *pep* and CNO neutrino rates within the measured or theoretical uncertainties changed the *pp* neutrino rate by less than 1%. We finally confirmed that the fit performed without constraining the ^{14}C rate returns a ^{14}C value consistent with the one previously measured independently (see above) and does not affect the *pp* neutrino result. The systematic errors are given in Table 1 for all fitted species.

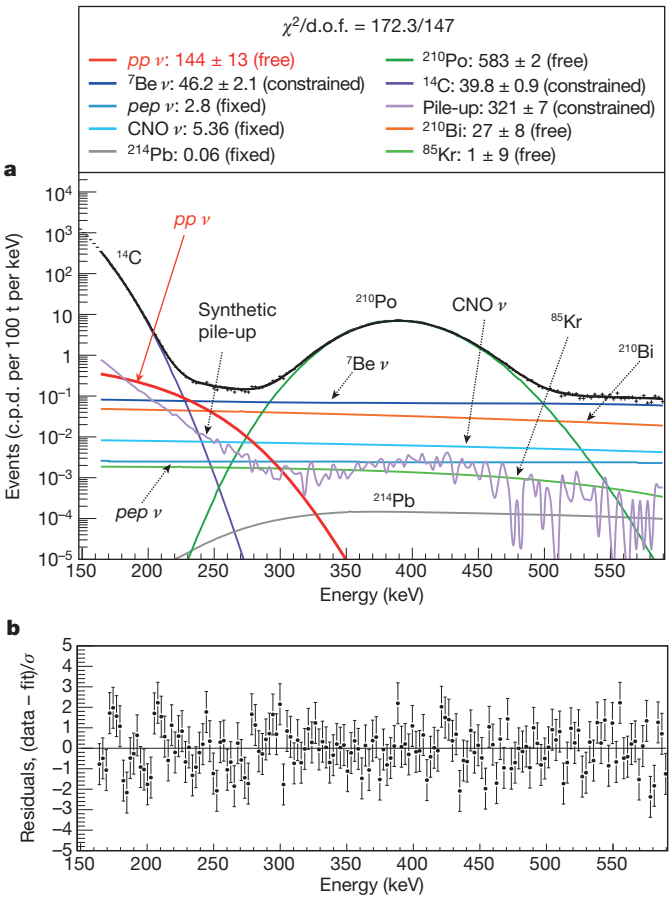

Figure 3 | Fit of the energy spectrum between 165 and 590 keV. a, The best-fit *pp* neutrino component is shown in red, the ^{14}C background in dark purple and the synthetic pile-up in light purple. The large green peak is ^{210}Po α-decays. ^{7}Be (dark blue), *pep* and CNO (light blue) solar neutrinos, and ^{210}Bi (orange) are almost flat in this energy region. The values of the parameters (in c.p.d. per 100 t) are in the inset above the figure. **b**, Residuals. Error bars, 1σ.

Table 1 | Results from the fit to the energy spectrum

Parameter	Rate ± statistical error (c.p.d. per 100 t)	Systematic error (c.p.d. per 100 t)
pp neutrino	144 ± 13	±10
^{85}Kr	1 ± 9	±3
^{210}Bi	27 ± 8	±3
^{210}Po	583 ± 2	±12

The best-fit value and statistical uncertainty for each component are listed together with its systematic error. The χ^2 per degree of freedom of the fit is χ^2/d.o.f. = 172.3/147.

We note that the very low ^{85}Kr rate (Table 1) is consistent with the independent limit (<7 c.p.d. per 100 t, 95% confidence level) obtained by searching for the β–γ delayed coincidence ^{85}Kr → ^{85m}Rb → ^{85}Rb (lifetime of the intermediate metastable isotope, $\tau = 1.46$ μs; branching ratio, 0.43%).

We have checked for possible residual backgrounds generated by nuclear spallation processes produced by cosmic ray muons that interact in the detector. We detect these muons with >99.9% efficiency[30]. We increased the time window for the muon veto from 300 ms to 5 s and observed no difference in the results. Furthermore, we searched for other possible background due to radioisotopes with sizeable natural abundances and sufficiently long half-lives to survive inside the detector over the timescale of this measurement. These include low-energy α-emitters such as ^{222}Rn and ^{218}Po (both belonging to the radon decay chain), ^{147}Sm and ^{148}Sm, and β-emitters (^{7}Be), which are all estimated to be negligible and are excluded from the final fit. One β-emitter, ^{87}Rb (half-life, $t_{1/2} = 4.7 \times 10^{10}$ yr; 28% isotopic abundance; $Q = 283.3$ keV), is of particular concern because of the relatively high abundance of Rb in the Earth's crust. Rubidium is an alkali chemically close to potassium but typically 2,000–4,000 times less abundant in the crust. Under these assumptions, and using the measured ^{40}K ($t_{1/2} = 0.125 \times 10^{10}$ yr; 0.0117% isotopic abundance) activity in the fiducial volume, that is, <0.4 c.p.d. per 100 t at the 95% confidence level[18], the ^{87}Rb activity in the Borexino scintillator can be constrained to be much less than 0.1 c.p.d. per 100 t, which is negligible for this analysis. A deviation from the crustal isotopic ratio by a factor of 100 would still keep this background at ~1 c.p.d. per 100 t.

The solar *pp* neutrino interaction rate measured by Borexino is 144 ± 13 (stat.) ± 10 (syst.) c.p.d. per 100 t. The stability and robustness of the measured *pp* neutrino interaction rate was verified by performing fits with a wide range of different initial conditions. The absence of *pp* solar neutrinos is excluded with a statistical significance of 10σ (Methods). Once statistical and systematic errors are added in quadrature and the latest values of the neutrino oscillation parameters[25] are taken into account, the measured solar *pp* neutrino flux is $(6.6 \pm 0.7) \times 10^{10}$ cm^{-2} s^{-1}. This value is in good agreement with the SSM prediction[9] ($5.98 \times (1 \pm 0.006) \times 10^{10}$ cm^{-2} s^{-1}). It is also consistent with the flux calculated by performing a global analysis of all existing solar neutrino data, including the ^{8}B, ^{7}Be and *pep* fluxes and solar neutrino capture rates[31,32]. Finally, the probability that *pp* neutrinos produced in the core of the Sun are not transformed into muon or tau neutrinos by the neutrino oscillation mechanism is found to be $P(\nu_e \rightarrow \nu_e) = 0.64 \pm 0.12$, providing a constraint on the Mikheyev–Smirnov–Wolfenstein large-mixing-angle (MSW-LMA) solution[25,33,34] in the low-energy vacuum regime (Methods).

Outlook

The proton–proton fusion reaction in the core of the Sun is the keystone process for energy production in the Sun and in Sun-like stars. The observation of the low-energy (0–420 keV) *pp* neutrinos produced in this reaction was possible because of the unprecedentedly low level of radioactivity reached inside the Borexino detector. The measured value is in very good agreement with the predictions of both the high-metallicity and the low-metallicity SSMs. Although the experimental uncertainty does not yet allow the details of these models to be distinguished, this measurement strongly confirms our understanding of the Sun. Future Borexino-inspired experiments might be able to measure solar *pp* neutrinos with the level of precision (~1%) needed to cross-compare photon

and neutrino solar luminosities, while providing insight into solar dynamics over 10^5-yr timescales. At the same time, such a precise measurement of *pp* neutrinos would yield the ultimate test for the MSW-LMA neutrino oscillation model and allow precision tests for exotic neutrino properties[35].

Online Content Methods, along with any additional Extended Data display items and Source Data, are available in the online version of the paper; references unique to these sections appear only in the online paper.

Received 20 April; accepted 18 July 2014.

1. Bethe, H. A. & Critchfield, C. L. The formation of deuterons by proton combination. *Phys. Rev.* **54,** 248–254 (1938).
2. Bethe, H. A. Energy production in stars. *Phys. Rev.* **55,** 434–456 (1939).
3. von Weizsäcker, C. F. Über Elementumwandlungen im Innern der Sterne. *Phys. Z.* **38,** 176–191 (1937).
4. Fowler, W. A. Completion of the proton-proton reaction chain and the possibility of energetic neutrino emission by hot stars. *Astrophys. J.* **127,** 551–556 (1958).
5. Cameron, A. W. G. Nuclear astrophysics. *Annu. Rev. Nucl. Sci.* **8,** 299–326 (1958).
6. Adelberger, E. G. *et al.* Solar fusion cross sections II: the *pp* chain and CNO cycles. *Rev. Mod. Phys.* **83,** 195–245 (2011).
7. Bahcall, J. N., Gonzalez-Garcia, M. C., & Peña-Garay, C. Does the Sun shine by *pp* or CNO fusion reactions? *Phys. Rev. Lett.* **90,** 131301 (2003).
8. Haxton, W. & Serenelli, A. CN-cycle solar neutrinos and the Sun's primordial core metallicity. *Astrophys. J.* **687,** 678–691 (2008).
9. Serenelli, A. M., Haxton, W. C. & Peña-Garay, C. Solar models with accretion - I. Application to the solar abundance problem. *Astrophys. J.* **743,** 24 (2011).
10. Anselmann, P. *et al.* (GALLEX Collaboration). Solar neutrinos observed by GALLEX at Gran Sasso. *Phys. Lett. B* **285,** 376–389 (1992).
11. Krauss, L. M. Reopening the solar neutrino question. *Nature* **357,** 437 (1992).
12. Abdurashitov, J. N. *et al.* Results from SAGE (the Russian-American solar neutrino gallium experiment). *Phys. Lett. B* **328,** 234–248 (1994).
13. Cleveland, B. T. *et al.* Measurement of the solar electron neutrino flux with the Homestake chlorine detector. *Astrophys. J.* **496,** 505–526 (1998).
14. Fukuda, Y. *et al.* Solar neutrino data covering solar cycle 22. *Phys. Rev. Lett.* **77,** 1683–1686 (1996).
15. Abe, Y. *et al.* (SuperKamiokande Collaboration). Solar neutrino results in SuperKamiokande-III. *Phys. Rev. D* **83,** 052010 (2011).
16. Ahmad, Q. R. *et al.* (SNO Collaboration). Measurement of the rate of $\nu_e + d \rightarrow p + p + e^-$ interactions produced by ^8B solar neutrinos at the Sudbury Neutrino Observatory. *Phys. Rev. Lett.* **87,** 071301 (2001).
17. Bellini, G. *et al.* (Borexino Collaboration). Precision measurement of the ^{7}Be solar neutrino interaction rate in Borexino. *Phys. Rev. Lett.* **107,** 141302 (2011).
18. Bellini, G. *et al.* (Borexino Collaboration). First evidence of *pep* solar neutrinos by direct detection in Borexino. *Phys. Rev. Lett.* **108,** 051302 (2012).
19. Bellini, G. *et al.* (Borexino Collaboration). Measurement of the solar ^{8}B neutrino rate with a liquid scintillator target and 3 MeV energy threshold in the Borexino detector. *Phys. Rev. D* **82,** 033006 (2010).
20. McDonald, A. SNO and future solar neutrino experiments. *Nucl. Phys. B Proc. Suppl.* **235–236,** 61–67 (2013).
21. Mitalas, R. & Sills, K. R. On the photon diffusion time scale for the Sun. *Astrophys. J.* **401,** 759–760 (1992).
22. Alimonti, G. *et al.* The Borexino detector at the Laboratori Nazionali del Gran Sasso. *Nucl. Instrum. Methods A* **600,** 568–593 (2009).
23. Bahcall, J. N. Gallium solar neutrino experiments: absorption cross sections, neutrino spectra, and predicted event rates. *Phys. Rev. C* **56,** 3391–3409 (1997).
24. Turck-Chièze, S. *et al.* Solar neutrinos, helioseismology and the solar internal dynamics. *Rep. Prog. Phys.* **74,** 086901 (2011).
25. Beringer J. *et al.* (Particle Data Group). Review of particle physics. *Phys. Rev. D* **86,** 010001 (2012); and 2013 partial update for the 2014 edition.
26. Bahcall, J. N., Kamionkowski, M. & Sirlin, A. Solar neutrinos: radiative corrections in neutrino-electron scattering experiments. *Phys. Rev. D* **51,** 6146–6158 (1995).
27. Kuzminov, V. V. & Osetrova, N. Ja. Precise measurement of ^{14}C beta spectrum by using a wall-less proportional counter. *Phys. At. Nucl.* **63,** 1292–1296 (2000).
28. Bellini, G. *et al.* (Borexino Collaboration). Final results of Borexino Phase-I on low-energy solar neutrino spectroscopy. *Phys. Rev. D* **89,** 112007 (2014).
29. Back H. . *et al.* Borexino calibrations: hardware, methods and results. *J. Instrum.* **7,** P10018 (2012).
30. Bellini G. *et al.* Muon and cosmogenic neutron detection in Borexino. *J. Instrum.* **6,** P05005 (2012).
31. Arpesella, C. *et al.* (Borexino Collaboration). Direct measurement of the ^{7}Be solar neutrino flux with 192 days of Borexino data. *Phys. Rev. Lett.* **101,** 091302 (2008).
32. Ianni, A. Solar neutrinos and the solar model. *Phys. Dark Univ.* **4,** 44–49 (2014).
33. Wolfenstein, L. Neutrino oscillations in matter. *Phys. Rev. D* **17,** 2369–2374 (1978).
34. Mikheyev, S. P. & Smirnov, A. Yu. Resonant amplification of neutrino oscillations in matter and spectroscopy of solar neutrinos. *Sov. J. Nucl. Phys.* **42,** 913–917 (1985).
35. Haxton, W. C., Robertson, R. G. H. & Serenelli, A. M. Solar neutrinos: status and prospects. *Annu. Rev. Astron. Astrophys.* **51,** 21–61 (2013).

Acknowledgements The Borexino program is made possible by funding from the INFN (Italy); the NSF (USA); the BMBF, DFG and MPG (Germany); the JINR; the RFBR, RSC and NRC Kurchatov Institute (Russia); and the NCN (Poland). We acknowledge the support of the Laboratori Nazionali del Gran Sasso (Italy).

Author Contributions The Borexino detector was designed, constructed and commissioned by the Borexino Collaboration over the span of more than 15 years. The Borexino Collaboration sets the science goals. Scintillator purification and handling, source calibration campaigns, PMT and electronics operations, signal processing and data acquisition, Monte Carlo simulations of the detector, and data analyses were performed by Borexino Collaboration members, who also discussed and approved the scientific results. The manuscript was prepared by a subgroup of authors appointed by the collaboration and subject to an internal collaboration-wide review process. All authors reviewed and approved the final version of the manuscript.

Author Information Reprints and permissions information is available at www.nature.com/reprints. The authors declare no competing financial interests. Readers are welcome to comment on the online version of the paper. Correspondence and requests for materials should be addressed to O.S. (borex-spokeperson@lngs.infn.it).

Borexino Collaboration G. Bellini[1], J. Benziger[2], D. Bick[3], G. Bonfini[4], D. Bravo[5], B. Caccianiga[1], L. Cadonati[6], F. Calaprice[7,8], A. Caminata[9], P. Cavalcante[4], A. Chavarria[7], A. Chepurnov[10], D. D'Angelo[1], S. Davini[11], A. Derbin[12], A. Empl[11], A. Etenko[13,14], K. Fomenko[4,15], D. Franco[16], F. Gabriele[4], C. Galbiati[7], S. Gazzana[4], C. Ghiano[9], M. Giammarchi[1], M. Göger-Neff[17], A. Goretti[7], M. Gromov[10], C. Hagner[3], E. Hungerford[11], Aldo Ianni[4], Andrea Ianni[7], V. Kobychev[18], D. Korablev[15], G. Korga[11], D. Kryn[16], M. Laubenstein[4], B. Lehnert[19], T. Lewke[17], E. Litvinovich[13,14], F. Lombardi[4], P. Lombardi[1], L. Ludhova[1], G. Lukyanchenko[13], I. Machulin[13,14], S. Manecki[5], W. Maneschg[20], S. Marcocci[8,9], Q. Meindl[17], E. Meroni[1], M. Meyer[3], L. Miramonti[1], M. Misiaszek[21], M. Montuschi[4], P. Mosteiro[7], V. Muratova[12], L. Oberauer[17], M. Obolensky[16], F. Ortica[22], K. Otis[6], M. Pallavicini[9], L. Papp[5,17], L. Perasso[9], A. Pocar[6], G. Ranucci[1], A. Razeto[4], A. Re[1], A. Romani[22], N. Rossi[4], R. Saldanha[7], C. Salvo[9], S. Schönert[17], H. Simgen[20], M. Skorokhvatov[13,14], O. Smirnov[15], A. Sotnikov[15], S. Sukhotin[13], Y. Suvorov[4,13,23], R. Tartaglia[4], G. Testera[9], D. Vignaud[16], R. B. Vogelaar[5], F. von Feilitzsch[17], H. Wang[23], J. Winter[24], M. Wojcik[21], A. Wright[7], M. Wurm[24], O. Zaimidoroga[15], S. Zavatarelli[9], K. Zuber[19] & G. Zuzel[21]

Affiliations for participants: [1]Dipartimento di Fisica, Università degli Studi e INFN, 20133 Milano, Italy. [2]Chemical Engineering Department, Princeton University, Princeton, New Jersey 08544, USA. [3]Institut für Experimentalphysik, Universität Hamburg, 22761 Hamburg, Germany. [4]INFN Laboratori Nazionali del Gran Sasso, 67100 Assergi, Italy. [5]Physics Department, Virginia Polytechnic Institute and State University, Blacksburg, Virginia 24061, USA. [6]Physics Department, University of Massachusetts, Amherst, Massachusetts 01003, USA. [7]Physics Department, Princeton University, Princeton, New Jersey 08544, USA. [8]Gran Sasso Science Institute (INFN), 67100 L'Aquila, Italy. [9]Dipartimento di Fisica, Università degli Studi e INFN, 16146 Genova, Italy. [10]Lomonosov Moscow State University Skobeltsyn Institute of Nuclear Physics, 119234 Moscow, Russia. [11]Department of Physics, University of Houston, Houston, Texas 77204, USA. [12]St Petersburg Nuclear Physics Institute, 188350 Gatchina, Russia. [13]NRC Kurchatov Institute, 123182 Moscow, Russia. [14]National Research Nuclear University MEPhI (Moscow Engineering Physics Institute), 115409 Moscow, Russia. [15]Joint Institute for Nuclear Research, 141980 Dubna, Russia. [16]APC, Université Paris Diderot, CNRS/IN2P3, CEA/Irfu, Observatoire de Paris, Sorbonne Paris Cité, 75205 Paris Cedex 13, France. [17]Physik-Department and Excellence Cluster Universe, Technische Universität München, 85748 Garching, Germany. [18]Kiev Institute for Nuclear Research, 03680 Kiev, Ukraine. [19]Department of Physics, Technische Universität Dresden, 01062 Dresden, Germany. [20]Max-Planck-Institut für Kernphysik, 69117 Heidelberg, Germany. [21]M. Smoluchowski Institute of Physics, Jagiellonian University, 30059 Krakow, Poland. [22]Dipartimento di Chimica, Biologia e Biotecnologie, Università degli Studi e INFN, 06123 Perugia, Italy. [23]Physics and Astronomy Department, University of California Los Angeles (UCLA), Los Angeles, California 90095, USA. [24]Institut für Physik, Johannes Gutenberg Universität Mainz, 55122 Mainz, Germany.

METHODS

The Borexino detector. The detector (Extended Data Fig. 1) is located deep underground (3,800 m of water equivalent) at the Gran Sasso laboratory, in central Italy[22]. The active neutrino target, 278 t of ultrapure liquid scintillator (pseudocumene (1,2,4-trimethylbenzene) solvent with 1.5 g l^{-1} 2,5-diphenyloxazole (PPO) wavelength-shifting fluor), is contained inside a thin transparent nylon spherical vessel of 8.5 m diameter. Borexino detects solar neutrinos by measuring the energy deposited by recoiling electrons following neutrino–electron elastic scattering. The scintillator promptly converts the kinetic energy of electrons into photons, detected and converted into electronic signals (photoelectrons) by 2,212 PMTs mounted on a concentric 13.7 m-diameter stainless steel sphere (SSS). The interaction in the scintillator of ionizing particles, such as those resulting from radioactive decays inside the detector (that we call background), can mimic and cover the expected signal. Every effort was made to minimize radioactive contamination of the scintillator and all surrounding detector materials. (1) The scintillator was produced from crude oil with minimal amounts of ^{14}C isotopic contamination (a key feature for this particular analysis). (2) Borexino has developed specific purification techniques[36,37] for scintillator, water and all other detector components, implemented innovative cleaning procedures and operated a 4 t prototype, the Counting Test Facility[38]; all this made it possible to reduce the radioactive contamination in ^{238}U and ^{232}Th to less than 10^{-18} g per gram of liquid scintillator, a level never reached before[22]. The Counting Test Facility also proved that organic liquid scintillator produced from ancient and deep underground oil sources can yield a very low ^{14}C/^{12}C ratio[39]. (3) The volume between the nylon vessel and the SSS is filled with 889 t of ultrapure non-scintillating fluid, and acts as radiation shield for radioactivity emitted by the PMTs. A second, larger (11.5 m diameter) nylon sphere prevents radon and other radioactive contaminants from the PMTs and SSS from diffusing into the inner part of the detector. The sphere is immersed in a 2,100 t water Cherenkov detector for residual cosmic muons, which can induce background via spallation processes with the scintillator.

Solar electron neutrino survival probability. After the SNO experiment in 2001[16], the deficit of solar ν_e observed on Earth has been explained by the neutrino oscillation mechanism: these ν_e undergo lepton flavour transformation into ν_μ or ν_τ in a quantum mechanical process requiring neutrinos to have a finite mass difference. The exact phenomenon is somewhat more complex (see ref. 35 for a recent review): beyond the neutrino oscillation mechanism in vacuum itself, there is a specific feature coming from matter effects while the neutrinos travel inside the Sun (the MSW effect[33,34]). This effect is energy dependent and is fully effective for solar neutrinos above ~5 MeV. Below 1 MeV, vacuum oscillations dominate, and a smooth transition region is predicted between ~1 and ~5 MeV. One of the parameters of oscillation is one of the three mixing angles between the neutrino species, for which all experimental data (from solar neutrino or reactor antineutrino experiments) isolate one particular solution, called the large-mixing-angle (LMA) solution; the model describing the solar neutrino results is now called MSW-LMA. The Borexino data, which cover the full solar neutrino spectrum, make it possible to test the predictions of the MSW-LMA model in all oscillation regimes with the same detector. Extended Data Fig. 2 shows the probability $P(\nu_e \rightarrow \nu_e)$ that ν_e produced in the core of the Sun are not transformed into ν_μ or ν_τ via the neutrino oscillation mechanism. The violet band corresponds to the 1σ prediction of the MSW-LMA solution, using the most recent values for the oscillation parameters[25]. The survival probability for the *pp* neutrino data from the present paper is $P(\nu_e \rightarrow \nu_e) = 0.64 \pm 0.12$, calculated using the formula

$$P(\nu_e \rightarrow \nu_e) = \frac{R^{\mathrm{exp}} - \Phi^{\mathrm{SSM}} n_e \sigma_\mu}{\Phi^{\mathrm{SSM}} n_e (\sigma_e - \sigma_\mu)}$$

where $R^{\mathrm{exp}} = (167 \pm 19) \times 10^{-5}$ c.p.s. per 100 t is the experimental rate measured by Borexino, $\Phi^{\mathrm{SSM}} = 5.98 \times (1 \pm 0.006) \times 10^{10}$ cm^{-2} s^{-1} is the *pp* neutrino theoretical flux, $n_e = (3.307 \pm 0.003) \times 10^{31}$ is the number of electrons for 100 t of the Borexino scintillator, and $\sigma_e = 11.38 \times 10^{-46}$ cm^2 and $\sigma_\mu = 3.22 \times 10^{-46}$ cm^2 are respectively the ν_e and ν_μ integrated cross-sections over the *pp* neutrino spectrum (which include radiative corrections[25,26] (also P. Langacker and J. Erler, personal communication)).

All the other data points correspond to the previous Borexino results[17–19]. We observe excellent agreement between our results and the MSW-LMA theoretical curve.

The standard solar model and the *pp* neutrino flux. The predictions for the solar neutrino fluxes come from solar models developed by astrophysicists since the 1960s. The SSM[40,41] uses the simplest physical hypotheses and the best available physics input. It is assumed that energy is generated by nuclear reactions in the core of the star (see Extended Data Fig. 3 for the *pp* cycle) and is transported by radiation in the central part and by convection in the outer part. The basic evolution equation is the hydrostatic equilibrium between the outward radiative pressure force and the inward gravitational force. One ingredient of the model, the metallicity Z/X (content of heavy elements relative to hydrogen), is under discussion at present (see, for example, ref. 9): the most recent determination of Z/X (AGS09) gives a lower value than the previous one (GS98), but the corresponding predictions significantly disagree with the helioseismology observations. The measurement of all solar neutrino components, which differ between solar models in these two metallicity scenarios, could help resolve the issue. The most recent calculations are those of ref. 9 (other models, such as the one described in ref. 24, give similar results). The predictions for the *pp* neutrino flux on Earth are[9] $5.98 \times (1 \pm 0.006) \times 10^{10}$ cm^{-2} s^{-1} for the high-metallicity model and $6.03 \times (1 \pm 0.006) \times 10^{10}$ cm^{-2} s^{-1} for the low-metallicity model (there is a difference of less than 1%, and we use the flux for high metallicity throughout this paper). When combined with the latest values of the neutrino oscillation parameters[25], the SSM predicts 131 ± 2 c.p.d. per 100 t from *pp* neutrinos in Borexino. Neutrino oscillation parameters are key for translating the interaction rate measured in Borexino into a solar neutrino flux, as they provide the relative ratio between electron neutrinos and muon and tau neutrinos, which have different elastic scattering cross-section with electrons.

Event selection, position and energy reconstruction. The basic event selection cuts for solar neutrino analysis are (1) no coincidence with muon events[30] (a 300 ms veto is applied following muons crossing the scintillator and buffer volumes, and a 2 ms veto following muons crossing only the water tank) and (2) position reconstruction within the innermost volume of the detector (the fiducial volume). The second cut is necessary to eliminate background from radioactivity in the nylon vessels, the SSS and the PMTs; for this analysis, $R < 3.021$ m, $|z| < 1.67$ m (the geometrical centre of the sphere defines the origin of the coordinates x and y (in the horizontal plane) and z, as well as the origin from where, R, is measured).

A signal is recorded when more than a preset number of PMTs (25 until 15 February 2013, 20 thereafter) detect light within a 100 ns time window. Dedicated software then decides whether to classify this as a physics event or archive it as electronic noise or other instrumental effect. A ray-tracing algorithm triangulates photon arrival times at each struck PMT to determine the position of the event, which is assumed to be point-like.

The procedure to assign the correct energy to each event starts from the number of photoelectrons recorded by the PMTs. For β- and γ-events, the energy of an event is roughly proportional to the number of collected photoelectrons[42]. Notably, α-events display sizeable quenching of scintillation light, description of which is beyond the scope of this Article. The number of photons detected for a given type of event depends on its position, being maximal at the centre of the detector. We correct for this position dependence using a parameterized response obtained by calibrating the detector with known radioactive sources deployed at different positions. Source calibration data (mostly γ-ray emitters) are then used to tune Monte Carlo simulation software[28], allowing us to model the detector response correctly. These are in turn used to determine the energy response of the detector. We detect approximately 500 photoelectrons for a 1 MeV electron; this number progressively reduces as ageing, malfunctioning PMTs are taken offline.

A complete description of the data selection and analysis can be found in ref. 28, with some conditions relaxed specifically for this analysis. In particular, the energy threshold for acceptance of events used in this analysis was lowered with respect to previous analyses looking for higher-energy neutrino interactions. Also by contrast with what was done in previous measurements, no β-like selection condition (based on the different scintillation time profile of α- and β-particles) was used, as its relative efficiency for neutrino and background events could not be reliably evaluated at the lower energies characteristic of solar *pp* neutrino interactions.

Fit of the ^{14}C. The ^{14}C rate has been determined by looking at a sample of data in which the event causing the trigger is followed by a second event within the time acquisition window of 16 μs. This particular second-event selection bypasses threshold effects intrinsic to any self-triggering approach, clearly visible in Extended Data Fig. 4. The energy spectrum and its fit, using the theoretical ^{14}C β-emission shape[27], are shown in Extended Data Fig. 5. The ^{14}C spectrum fits the data well, yielding a ^{14}C rate of 40 ± 1 Bq per 100 t. The uncertainty accounts for systematic effects due to the stability of the detector response in time, knowledge of the ^{14}C spectral shape and fit conditions, including the fit energy range. We note that the relatively poorly known shape factor of the ^{14}C β-emission spectrum has a <2% effect on the *pp* neutrino result. The measured ^{14}C rate translates into a ^{14}C/^{12}C isotopic ratio of $(2.7 \pm 0.1) \times 10^{-18}$. The typical value for this ratio for atmospheric (that is, biologic) carbon is $\sim 10^{-12}$. ^{14}C is mainly produced by the nuclear reaction ^{14}N(n,p)^{14}C supported by cosmic rays in the upper atmosphere. The underground petroleum origin of the Borexino liquid scintillator explains its much smaller ^{14}C abundance.

Study of pile-up events. The pile-up component is determined using a data-driven method as follows. The real triggered events without any selection cuts are artificially overlapped with random data samples. The combined synthetic events are selected and reconstructed using the procedure applied to the regular data. By construction, the synthetic pile-up method accounts for all possible event pile-up

combinations. The corresponding spectrum includes events that vary in energy with respect to the original event (that is, before being artificially overlapped with the random sample) by more than a given number of photoelectrons (N_{min}). In addition, the same event selection criteria as in the real data set are applied after the overlap. Thus, some systematic effects, for example the position reconstruction of pile-up events, are automatically taken into account. To increase the statistical precision, every real event is overlapped four times, each time with a different random data sample, and the final pile-up spectrum is divided by a factor of 4. An expanded view of the synthetic pile-up spectral probability density function (visible in Figs 2 and 3) is presented in Extended Data Fig. 6.

The final fit was performed using this synthetic pile-up with $N_{min} = 5$ photoelectrons. This component is dominated but not exclusively composed of ^{14}C pile-up with itself. Some of the events are from dark noise of the PMTs. The robustness of the method was confirmed by checking that the fit results were not dependent on the choice of N_{min}.

We compared the synthetic pile-up method with an alternative one. Regularly solicited trigger events with a 16 μs acquisition time window (acquired at 0.5 Hz) are collected and sliced into fixed-time windows of the same duration as the signal window (230 and 400 ns). The hits in these windows produce the energy distribution shown in Extended Data Fig. 7, which represents a randomly sampled signal from the detector, including contributions from dark noise of the PMTs, ^{14}C and other radioactive contaminants. Pile-up can be thought of as the combination of events belonging to any spectral component combined with such a spectrum. The final fit can then be performed without a separate pile-up probability density function (as in the synthetic approach), by using 'smeared' spectral species in the final fit. The smearing is the convolution of ideal spectral components with the solicited trigger spectrum. Solar *pp* neutrino interaction rates measured using this method are in full agreement with those obtained with the synthetic pile-up method.

Stability of the result. The stability and robustness of the measured *pp* neutrino interaction rate was verified by performing fits with a wide range of different initial conditions, including fit energy range, synthetic-versus-convolution pile-up spectral shape, and energy estimator. The distribution of *pp* neutrino interaction rates obtained for all these fit conditions is summarized in Extended Data Fig. 8. The possibility of some remaining external background in the fiducial volume has been carefully studied in all Borexino solar neutrino analyses (see, for example, refs 17, 28). From these, we are confident that such a background at energies relevant for the *pp* neutrino study is negligible. In the particular case of the very low-energy part of the spectrum, we have tested this confidence by repeating the fit in five smaller fiducial volumes (with smaller radial and/or z-cut), which yields very similar results. Finally, the goodness (χ^2) of the spectral fit was computed using different values of the *pp* interaction rate, as shown in Extended Data Fig. 9. The absence of *pp* solar neutrinos is excluded with a statistical significance of 10σ.

36. Benziger, J. *et al.* A scintillator purification system for the Borexino solar neutrino detector. *Nucl. Instrum. Methods A* **587,** 277–291 (2008).
37. Alimonti, G. *et al.* The handling liquid systems for the Borexino solar neutrino detector. *Nucl. Instrum. Methods A* **609,** 58–78 (2009).
38. Alimonti, G. *et al.* (Borexino Collaboration). Ultra-low background measurements in a large volume underground detector. *Astropart. Phys.* **8,** 141–157 (1998).
39. Alimonti, G. *et al.* (Borexino Collaboration). Measurement of the ^{14}C abundance in a low-background liquid scintillator. *Phys. Lett. B* **422,** 349–358 (1998).
40. Bahcall, J. N. & Ulrich, R. K. Solar models, neutrino experiments and helioseismology. *Rev. Mod. Phys.* **60,** 297–372 (1988).
41. Bahcall, J. N. & Pinsonneault, M. H. Solar models with helium and heavy element diffusion. *Rev. Mod. Phys.* **67,** 781–808 (1995).
42. Knoll, G. F. *Radiation Detectors and Measurement* 4th edn, 290–291 (Wiley, 2010).

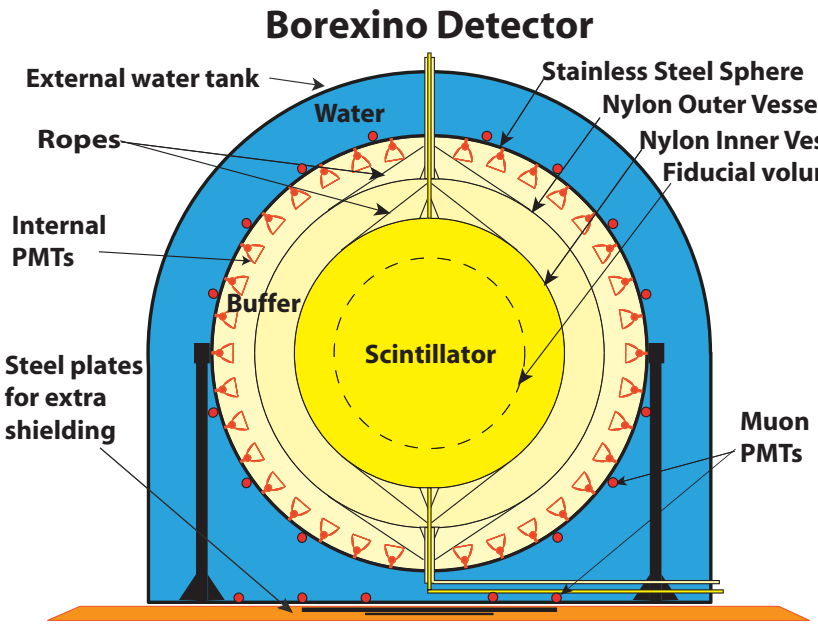

Extended Data Figure 1 | The Borexino detector. The characteristic onion-like structure of the detector[22] is displayed, with fluid volumes of increasing radiological purity towards the centre of the detector. Although solar neutrino measurements are made using events whose positions fall inside the innermost volume of scintillator (the fiducial volume, shown as spherical for illustrative purposes only), the large mass surrounding it is necessary to shield against environmental radioactivity. The water tank (17 m high) contains about 2,100 t of ultraclean water. The diameter of the stainless steel sphere is 13.7 m, and that of the thin nylon inner vessel containing the scintillator is 8.5 m. The buffer and target scintillator masses are 889 and 278 t, respectively.

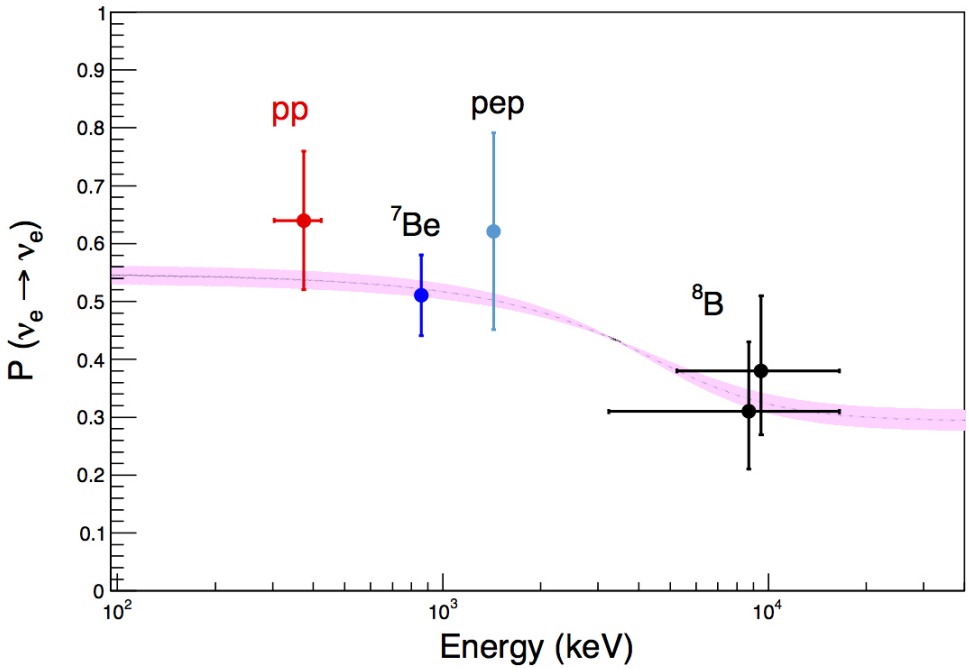

Extended Data Figure 2 | Survival probability of electron-neutrinos produced by the different nuclear reactions in the Sun. All the numbers are from Borexino (this paper for *pp*, ref. 17 for ^{7}Be, ref. 18 for *pep* and ref. 19 for ^{8}B with two different thresholds at 3 and 5 MeV). ^{7}Be and *pep* neutrinos are mono-energetic. *pp* and ^{8}B are emitted with a continuum of energy, and the reported $P(\nu_e \rightarrow \nu_e)$ value refers to the energy range contributing to the measurement. The violet band corresponds to the $\pm 1\sigma$ prediction of the MSW-LMA solution[25]. It is calculated for the ^{8}B solar neutrinos, considering their production region in the Sun which represents the other components well. The vertical error bars of each data point represent the $\pm 1\sigma$ interval; the horizontal uncertainty shows the neutrino energy range used in the measurement.

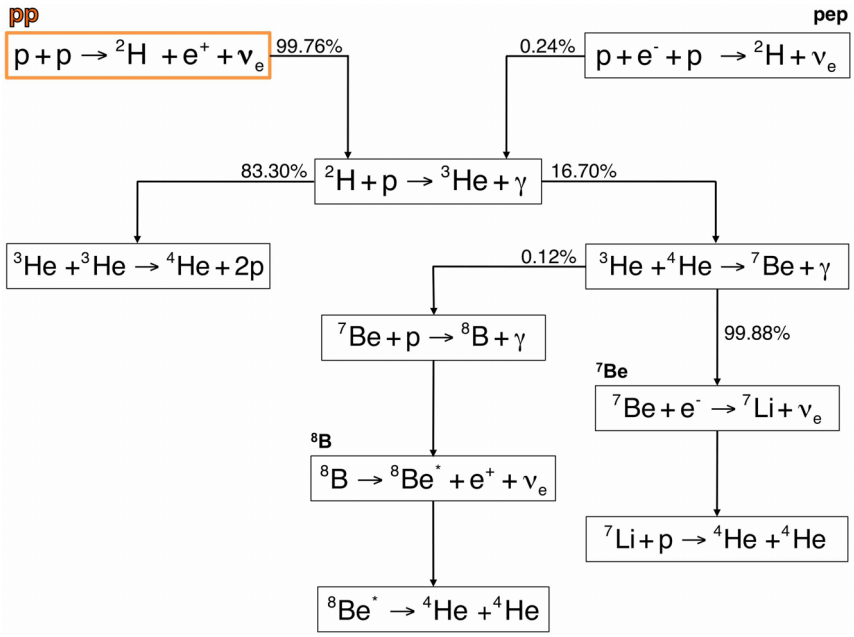

Extended Data Figure 3 | The sequence of nuclear fusion reactions defining the *pp* chain in the Sun. The *pp* neutrinos start the sequence 99.76% of the time.

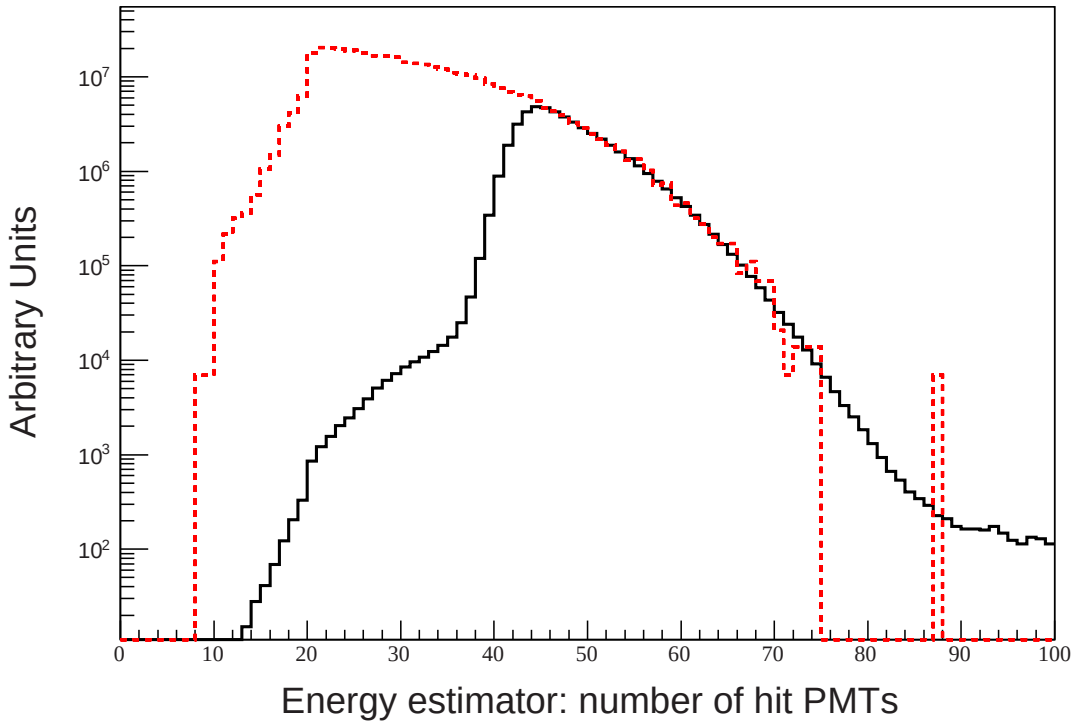

Extended Data Figure 4 | Study of the low energy part of the spectrum. Comparison of the spectrum obtained with the main trigger (black) and by selecting events falling in the late part of the acquisition window triggered by preceding events (red). Above 45 struck PMTs, the spectral shapes coincide. The threshold effect for self-triggered events (black) is clear. The residual threshold effect at lower energy in the red curve is due to the finite efficiency for identifying very low-energy events within a triggered data window.

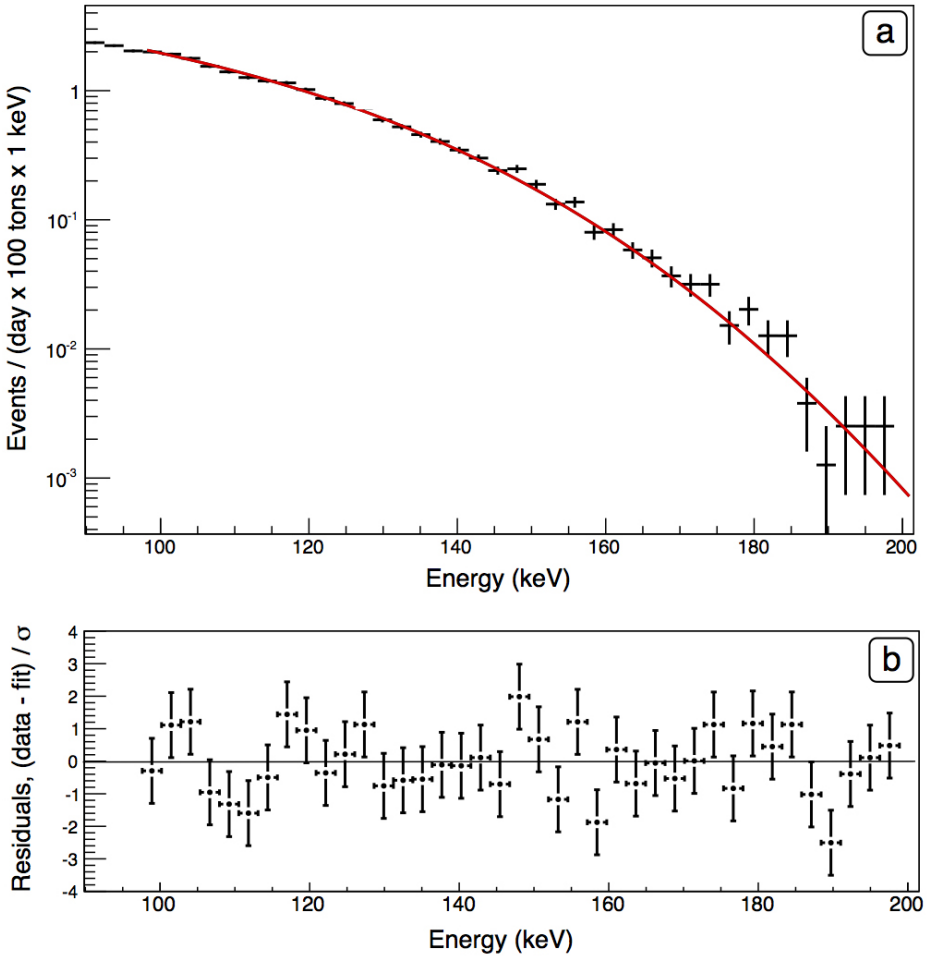

Extended Data Figure 5 | ^{14}C spectrum, and residuals, obtained from events triggered by a preceding event. **a**, Spectrum. **b**, Relative residuals of a fit with the ^{14}C β-emission spectrum (in units of standard deviations). The error bars thus represent $\pm 1\sigma$ intervals.

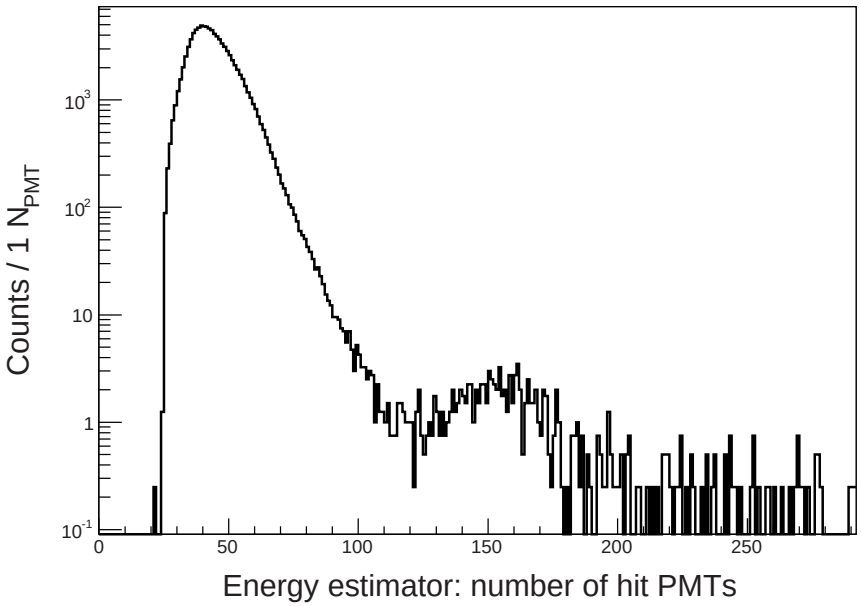

Extended Data Figure 6 | Energy spectrum of the pile-up data for the standard cuts. The small bump around 150 struck PMTs (~400 keV in Figs 2 and 3) is due to the pile-up of ^{14}C with ^{210}Po; at lower energies, pile-up is dominated by $^{14}C+^{14}C$, and by ^{14}C+dark noise.

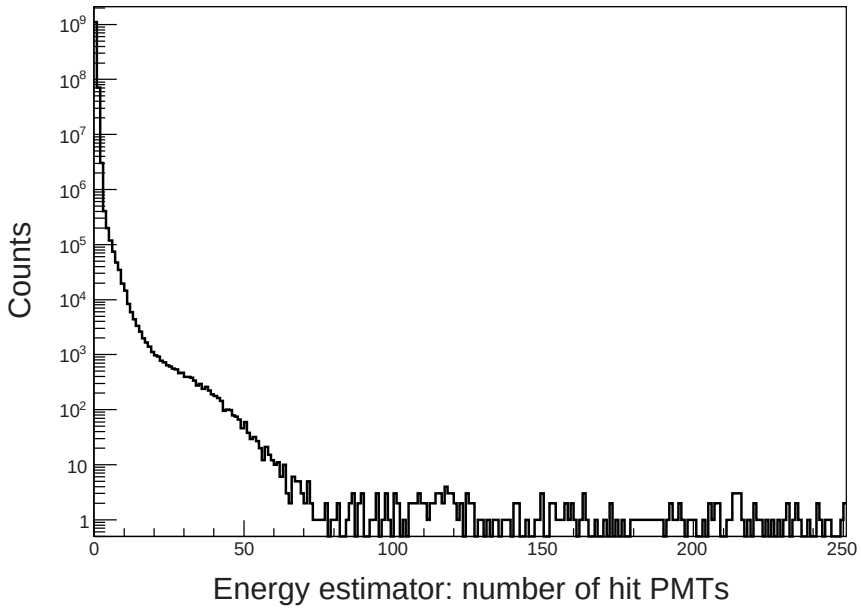

Extended Data Figure 7 | Energy distribution of events collected with no threshold applied. The events correspond to regular, solicited triggers (sliced into 230 ns windows). This represents what the detector measures when randomly sampled. In an alternative treatment of pile-up, this spectrum is used to smear each spectral component used in the fit (see text for details).

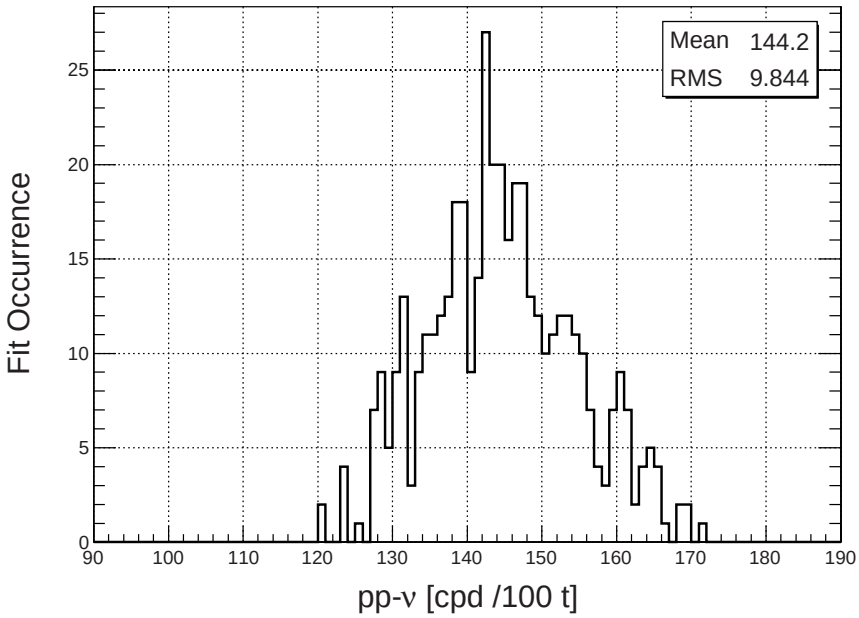

Extended Data Figure 8 | Distribution of best-fit values for the *pp* neutrino interaction rate. Values are obtained by varying the fit conditions, including the fit energy range, synthetic-versus-analytic pile-up spectral shape, and energy estimator. The distribution shown is peaked around our reported value of 144 c.p.d. per 100 t.

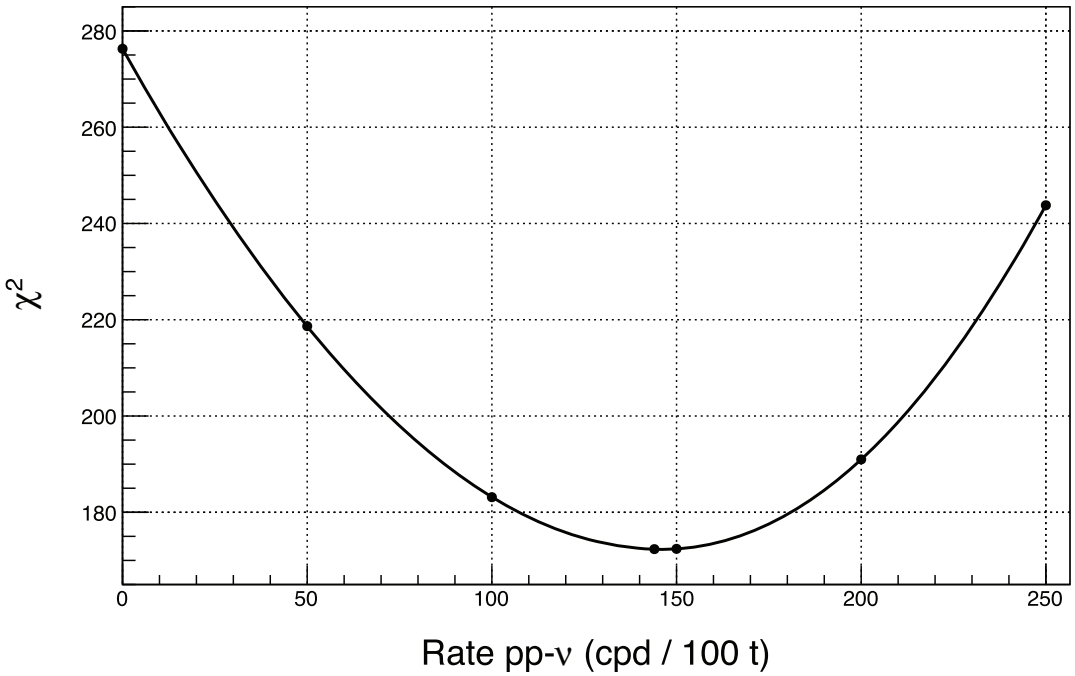

Extended Data Figure 9 | Goodness of fit versus *pp* neutrino interaction rate. The χ^2 minimum is at our reported value of 144 c.p.d. per 100 t.